Environmental Sensor Board

Imperial College London, Dep. of Electrical and Electronic Engineering,
ELEC70132 - Laboratory in Sensor Systems, Group 5

1. Environmental Sensor Board Overview

The original intention was to develop a single-PCB sensor system capable of wired and wireless communication (via a Wi-Fi connection). See Table 1 for details on the components present in this PCB. Note that all the relevant files for this project can be found in the public GitHub page: https://github.com/shenshang521/ELEC70132_Group5_Environment-sensor

Table 1. Components of Environmental Sensor

Component	Model
Microcontroller	Adafruit ESP32-S3 Feather
Gas Sensor	Adafruit BME688
GPS Tracker	Adafruit Mini GPS PA1010D
Time of Flight Sensor	Adafruit VL53L4CX
MicroSD Breakout	Adafruit MicroSD card breakout board+
Display	Adafruit Monochrome 0.96" 128x64 OLED Graphic Display

2. PCB Design and Sensor Integration

Schematic: the Environmental Sensor Board is built around the Adafruit ESP32-S3 Feather microcontroller. As shown in Figure 1, the PCB consists of numerous female header pins that accommodate all of the electronic components.

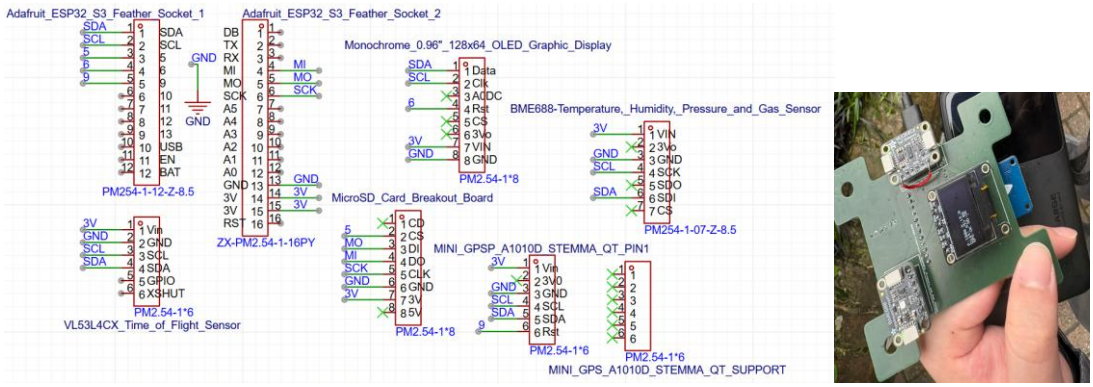

Figure 1. PCB Schematic View (Left) & Additional Jumper Connection (Right)

Note that after the PCB was manufactured and brief testing was done, it became apparent that there was a missing copper connection – for the STEMMAQT VL53L4CX Time of Flight sensor to be responsive, the XSHUT pin must be tied HIGH. However, this pin was left floating in the PCB design. To solve this in post-manufacture, a HIGH signal was sourced from the Vin pin which is indeed connected to 3.3V power – simply, a jumper wire was soldered between the Vin and the XSHUT pins of the sensor.

Note that the I2C protocol for data transfer to/ MCU is used by all of the on-board components, except for the microSD card breakout board – SPI communication is used for this. Also note that in terms of power, the board is powered through the USB port of the ESP32 microcontroller. The MCU then transfers this power to all the other components via its 3V pin. The MCU can be powered through various sources, such as a laptop USB port, a dedicated USB power bank, or any other USB-compatible power supply.

Layout: A compact two-sided layout was made, measuring only 84×96mm (see Figure 2). For better user experience, all components that require top-down openings on the enclosure were placed on the top side of the PCB (the BME688 Sensor, the Time-of-Flight sensor, and the OLED display). This way, the user can interact with the sensors and read the outputs on the OLED display without having to tilt the entire assembly with their hands. Openings for four M6 screws were included – these were made to accommodate M6 screws (the diameter of the holes was set to 6.2 mm to ensure clearance for the 6 mm diameter screws).

The two PCB layers had roughly the following purposes: top layer – signals, bottom layer – GND. The ground plane improves signal integrity by providing a low impedance return path and reduces electromagnetic interference (EMI) as it provides electromagnetic shielding.

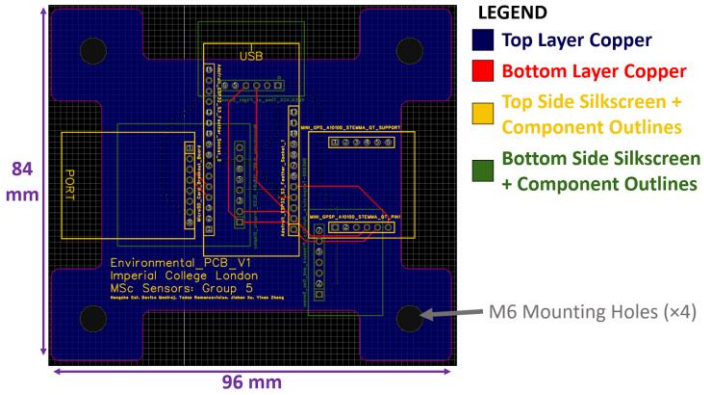

Figure 2. PCB Layout Design

I²C and SPI were the fastest signals on the PCB, so the traces were routed with extra care, mainly by keeping them well spaced to reduce crosstalk. Power traces were made wider (0.53 mm) for better current/thermal margin, while signal traces were kept narrower (0.254 mm) to save routing space.

For usability, the MCU USB connector and the SD card slot were placed on the PCB edges and faced outward for easy access.
A copper keep-out under the MCU's 2.4 GHz antenna was missed in the first revision and only noticed after manufacture. In practice, no obvious wireless issues were seen, likely because the MCU sat on 8.5 mm headers, creating enough separation from the PCB copper. Without this gap, the antenna could have been affected, and nearby traces might have picked up interference.

This PCB design successfully allowed for the entire assembly to be in operation – all the breakout boards present on the PCB can be powered and are capable of communication with the MCU. The M6 mounting holes also fitted screws successfully.

3. 3D Printed Enclosure

During the design process, it was kept in mind that the environmental sensing PCB is to be put inside a 3D printed enclosure. Therefore, relevant 3D models were downloaded (mostly from Snapmagic) and assigned to the corresponding components. This aided in the design of the 3D printed enclosure – see Figure 3.

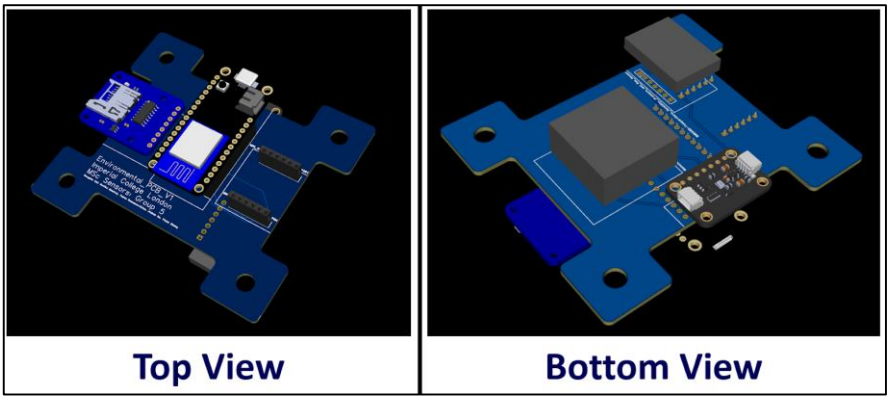

Figure 3. PCB 3D View with 3D Component Models/Outlines

A custom 3D-printed enclosure was designed using FreeCAD for the PCB (see Figure 4). The main purpose of the enclosure is to protect the circuit and prevent accidental contact with the components during operation. PLA was used as the printing material since it is easy to manufacture using standard 3D printers and provides enough strength for an indoor electronic system. The enclosure consists of a base and a lid, with the lid fixed in place using screws so that the PCB can be accessed easily if required.

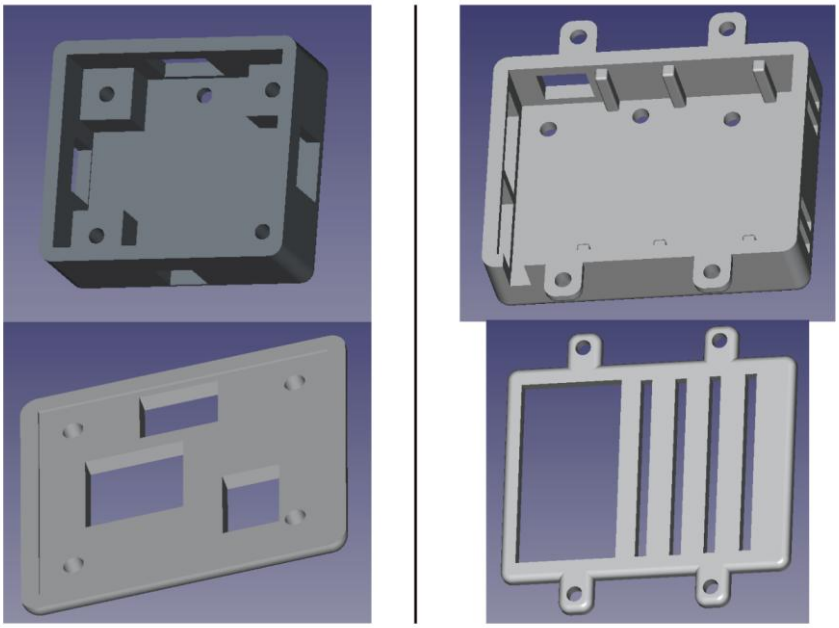

Figure 4. Left: Enclosure for PCB, Right: Enclosure for Power Bank

Openings were included in the enclosure based on the functional requirements of the PCB. Cut-outs are provided for the distance sensor, pressure sensor, and gas sensor, as these components need direct exposure to the surrounding environment for correct operation. An opening is also provided for the graphic OLED display so that system information can be viewed during use. In addition, a dedicated slot is included for the SD card, which is used to store data collected from the environmental sensors. This allows the SD card to be inserted or removed without opening the enclosure. Ventilation holes are added to reduce heat build-up during continuous operation.

A separate enclosure was designed for the power bank used to supply power to the system. This enclosure includes an opening for the power bank display and ventilation holes for heat dissipation. Both the PCB enclosure and the power bank enclosure include openings for USB cables, allowing them to be connected easily while keeping the overall setup compact and organised.

4. Data Collection and Comparison

4.1. Measurement Campaign

4.1.1. BME688

Field measurements took place on December 7, 2025, to assess the system's performance and the combined effect of the environment on public health. The study covered three distinct London sites, ranging from quiet indoor spaces to busy urban roads and healthcare facilities.

1) Indoor Control: EEE Building, Room 303 (Imperial College)

Public Health Relevance:

- Air Quality (VOCs): As a primary laboratory space, monitoring VOCs helps assess the risk of air quality which directly impacts cognitive function and long-term health.
- Thermal Comfort (Temp/Humidity): High humidity can promote mold growth and increase disease transmission rates, while deviations from the optimal room temperature range (20-24°C) can reduce concentration and productivity.

2) Urban Traffic Zone: Exhibition Road (South Kensington)

Public Health Relevance:

- Pollution Trapping (Pressure/VOCs): This is a shared space accommodating heavy vehicular traffic alongside tourists and students – air quality is highly of interest here.
- We also monitor Atmospheric Pressure, as high-pressure systems can lead to stagnant air, trapping pollutants at ground

level and introducing respiratory risks for pedestrians. [1]

3) Vulnerable Population Zone: Royal Brompton Hospital (Perimeter)

Public Health Relevance:

- Health Risks: Patients with cardiovascular and respiratory conditions are exceptionally vulnerable not just to pollution, but to meteorological extremes. [2]
- Cold/Damp Stress: High humidity combined with low temperatures is a known trigger for asthma and chronic obstructive pulmonary disease (COPD) exacerbations. [3] By monitoring these parameters alongside VOCs, we can assess whether the external environment can impact patient recovery.

4.1.2. Time of Flight

To verify the ranging accuracy and linearity of the VL53L4CX sensor, we conducted a distance measurement test. Experimental setup: The environmental sensor node was placed on an experimental platform. A standard metric ruler (resolution: ±1.0 mm) was parallel to the sensor's field of view (FoV) as a reference.

Test procedure: A human palm was used as the target object. The palm was placed flat and perpendicular to the sensor's optical path. The distance between the target object and the sensor varied between 50 mm and 500 mm (this is the typical effective range for gesture control). At each discrete location, the digital reading output of the VL53L4CX (via the I^2C interface) was recorded and compared with the physical measurement on the ruler. This comparison can identify any systematic bias or nonlinearity in the sensor's time-to-distance conversion algorithm.

4.1.3. GPS

An Adafruit Mini GPS PA1010D module was integrated to add location tags to environmental readings, enabling air-quality variations to be mapped to specific areas. The module outputs standard NMEA messages, providing latitude/longitude and UTC time, with UTC serving as a common time reference for synchronizing records. A 1 Hz update rate was selected as a balance between oversampling and undersampling: it is sufficient to track walking-speed movement while avoiding excessive SD-card write load. To maintain data quality, location data is only logged when the receiver reports a valid 3D location, preventing invalid or blank coordinates during startup or when signal is lost (e.g., indoors).

4.2. Data Storage and Retrieval Architecture

A dual-mode system is designed to make sure we never lose data and can access it easily without taking the device apart.

1) **Local backup (microSD logging): s**ensor readings are stored on an onboard microSD card as CSV files, allowing direct import into tools such as Excel or MATLAB. To align measurements with real-world events, the MCU synchronises its clock over WiFi using Network Time Protocol (NTP), so each record is stored with an accurate timestamp. Importantly, SD logging remains independent of WiFi, ensuring continuous recording even if wireless connectivity is unavailable or disabled to save power.
2) **Wireless Telemetry Interface (Web-Based Dashboard):** the node hosts a lightweight web interface accessible from a phone or laptop browser, meaning the SD card does not need to be removed for data access. The dashboard provides live sensor readouts for in-field verification, supports wireless download of the full CSV log over the local network, and includes a remote reset/clear function to prepare the device quickly for subsequent measurement runs.

5. Results & Comparison

Table 2. BME688 Test Results

	EEE building 303	Exhibition Road	Brompton Hospital	Official Data (Weather Underground)
Temperature(°C)	25.2	14	16.7	11.4
Humidity (%)	44	77	74	79
Pressure (hPa)	1006	1000	1000	1000
Air Quality (%)	50	27	24	none (uses different scale)

Table 3. Time-of-Flight Sensor Test Results

Ruler	10mm	30mm	50mm
TOF output	9mm	28mm	52mm

Table 4. GPS Test Results

Measurement Site	Environment Type	Recorded Coordinates (Sensor Node)	Reference Coordinates (Google Maps)	Deviation / Status
EEE Building (Room 303)	Indoor Control	*No Fix (0.00, 0.00)*	51.4988° N, 0.1749° W	Signal Blocked: Attenuation by building structure.
Exhibition Road	Urban Traffic	51.4963° N, 0.1741° W	51.4965° N, 0.1743° W	≈ 15m Error: Acceptable for zone identification.
Brompton Hospital	Sensitive Perimeter	51.4891° N, 0.1712° W	51.4895° N, 0.1710° W	≈ 25m Error: Affected by Urban Canyon effect.

6. Discussion & Critical Analysis

Environmental Sensor Analysis (BME688): The data comparison reveals that while the indoor air (in EEE303) had higher quality (50%), the outdoor readings at Exhibition Road and Brompton Hospital dropped significantly to 27% and 24%, respectively. Traffic emissions contribute to this. Though error sources should also be considered. An error to the air quality measurement is introduced by humidity interference – the BME688 detects VOCs by measuring the resistance of a metal-oxide layer; high ambient humidity introduces water molecules that increase conductivity, lowering the resistance and causing a "false positive" for pollution. Furthermore, the recorded temperatures were higher than the official meteorological data, suggesting heat accumulation within the 3D-printed enclosure generated by the electronics may also affect the readings of the sensor.

Time-of-Flight Sensor Analysis (VL53L4CX): The ToF sensor demonstrated high linearity but exhibited minor absolute errors ranging from -2mm to +2mm compared to the reference ruler. These deviations are attributed to the target properties used in the validation (a human palm). Unlike the rigid, flat surface of a purpose-specific calibration card, human skin has a lower IR reflectivity and a non-uniform texture, which can reduce the signal-to-noise ratio of the returning EM signal. Additionally, unavoidable micro-movements of the hand during measurement introduce dynamic instability.

GPS Analysis: A position error of about 15–25 m was observed when comparing the logged GPS points with the real locations on the map. In central London this is not surprising: tall buildings around Exhibition Road can block satellite signals, and reflections from glass and concrete can cause the position estimated by the receiver to be slightly away from the true position. Although the outdoor error is considerable, it is expected for this project. The goal was to tell apart large areas (e.g., “hospital area” vs “main road”), which are separated by much more than 25m, so the GPS accuracy was sufficient to assign measurements to the correct general area. Inside the EEE Building, the GPS receiver could not get a location fix at all, which shows that GPS works well outdoors but is unreliable indoors because the satellite signal gets attenuated too strongly when passing through thick walls of the building. Indoor tracking with this device would therefore need another method (e.g., WiFi-based positioning).

7. References

[1] F. J. Kelly and J. C. Fussell, “Air Pollution and Public health: Emerging Hazards and Improved Understanding of Risk,” Environmental Geochemistry and Health, vol. 37, no. 4, pp. 631–649, Jun. 2015, doi: https://doi.org/10.1007/s10653-015-9720-1. Available: https://link.springer.com/article/10.1007/s10653-015-9720-1

[2] S. C. Anenberg, S. Haines, E. Wang, N. Nassikas, and P. L. Kinney, “Synergistic health effects of air pollution, temperature, and pollen exposure: a systematic review of epidemiological evidence,” Environmental Health: A Global Access Science Source, vol. 19, no. 1, pp. 1–19, Dec. 2020, doi: https://doi.org/10.1186/s12940-020-00681-z. Available: http://web.b.ebscohost.com/ehost/detail/detail?vid=3&sid=38b41624-3d27-407a-a448-a299a0d05113%40sessionmgr101&bdata=JkF1dGhUeXBlPWNvb2tpZSxpcCx1cmwsY3BpZCZjdXN0aWQ9czg5MzMzNTkmc2l0ZT1laG9zdC1saXZl#AN=147454777&db=a9h

[3] S. Mekhuri, S. Quach, C. Barakat, W. Sun, and M. L. Nonoyama, “A cross-sectional survey on the effects of ambient temperature and humidity on health outcomes in individuals with chronic respiratory disease,” Canadian journal of respiratory therapy, vol. 59, Dec. 2023, doi: https://doi.org/10.29390/001c.90653. Available: https://www.ncbi.nlm.nih.gov/pmc/articles/PMC10710831/

Appendix A:

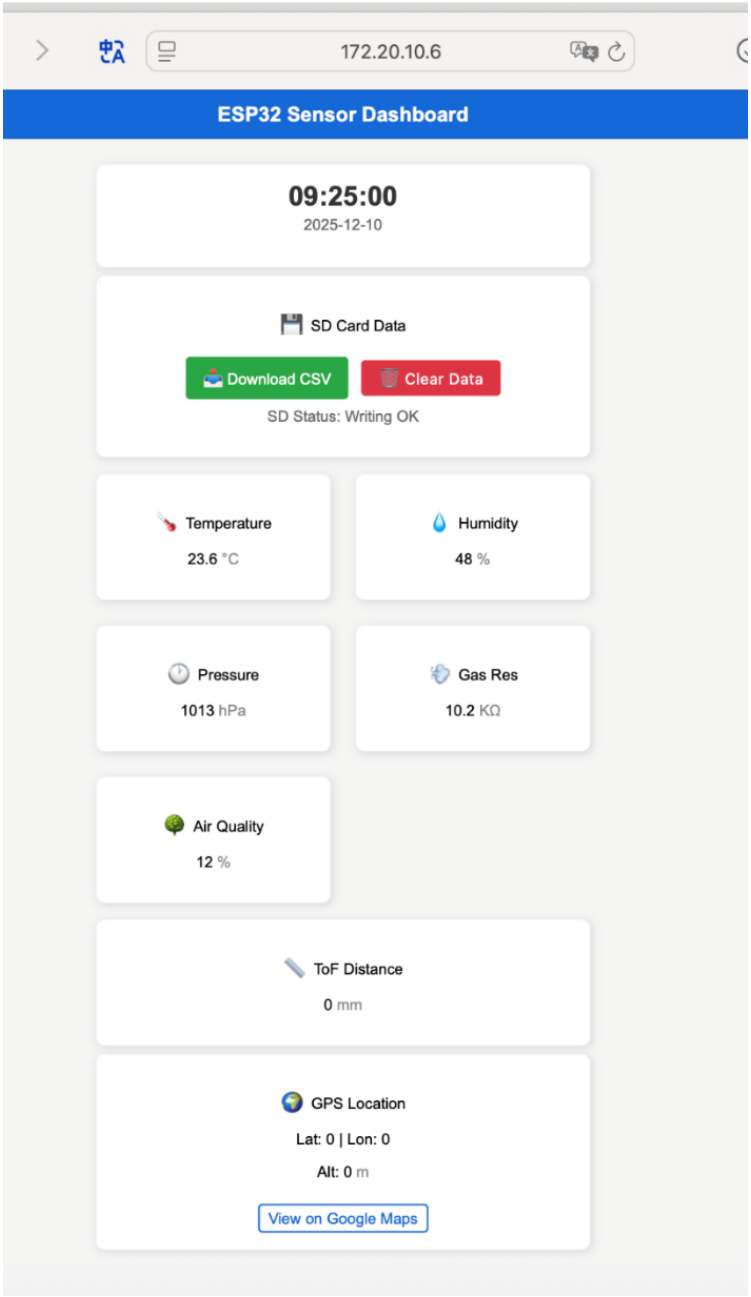

Figure 5. Screenshot of Web-Based Dashboard

Figure 6. Left: Environmental Board displaying Data. Right: Test Location for the Royal Brompton Hospital